

---

# DP-LDMs: Differentially Private Latent Diffusion Models

---

Saiyue Lyu<sup>\*1</sup> Michael F. Liu<sup>\*1</sup> Margarita Vinaroz<sup>\*23</sup> Mijung Park<sup>4</sup>

## Abstract

Diffusion models (DMs) are one of the most widely used generative models for producing high quality images. However, a flurry of recent papers points out that DMs are least private forms of image generators, by extracting a significant number of near-identical replicas of training images from DMs. Existing privacy-enhancing techniques for DMs, unfortunately, do not provide a good privacy-utility tradeoff. To address this challenge, a recent paper suggest pre-training DMs with public data, then fine-tuning them with private data using DP-SGD for a relatively short period. In this paper, we further improve the current state of DMs with differential privacy (DP) by adopting the *Latent* Diffusion Models (LDMs). LDMs are equipped with powerful pre-trained autoencoders that map the high-dimensional pixels into lower-dimensional latent representations, in which DMs are trained, yielding a more efficient and fast training of DMs. Rather than fine-tuning the entire LDMs, we fine-tune only the *attention* modules of LDMs with DP-SGD, reducing the number of trainable parameters by roughly 90% and achieving a better privacy-accuracy trade-off. Our approach allows us to generate realistic, high-dimensional images (256x256) conditioned on text prompts with DP guarantees, which, to the best of our knowledge, has not been attempted before. Our approach provides a promising direction for training more powerful, yet training-efficient differentially private DMs, producing high-quality DP images.

## 1. Introduction

A flurry of recent work highlights the tension between increasingly powerful diffusion models and data privacy, e.g., (Wu et al., 2023; Carlini et al., 2023; Tang et al., 2023; Hu & Pang, 2023; Duan et al., 2023; Matsumoto et al., 2023; Somepalli et al., 2023) among many. These papers commonly conclude that diffusion models are extremely good at memorizing training data, leaking more than twice as much training data as GANs (Carlini et al., 2023). This raises the question on how diffusion models should be responsibly deployed.

To tackle the privacy concerns, Dockhorn et al. (2023) propose to use DP-SGD (Abadi et al., 2016) when training DMs. However, DP trained DMs yield rather underwhelming performance when evaluated on datasets such as CIFAR10 and CelebA. Recently, Ghalebikesabi et al. (2023) propose to pretrain a large diffusion-based generator using public data, then fine-tune it with private data for a relatively small number of epochs using DP-SGD. This method currently achieves state-of-the-art performance on CIFAR10 images generated from DP-fine-tuned DMs.

In this paper, our goal is to further improve the performance of DP-fine-tuned DMs. To achieve this, we build on *latent diffusion models (LDMs)* (Rombach et al., 2022), which uses a pre-trained autoencoder to map the high-dimensional pixels to the so-called *latent variables*, which enter into the diffusion model. The latent diffusion model defined on the lower-dimensional latent space has a significantly lower number of parameters to fine-tune than the diffusion model defined on the pixel space. Rather than fine-tuning entire LDM, we choose to fine-tune only the *attention modules* (and *conditioning embedders* for conditional generation) in the LDM using DP-SGD. As a result, the number of trainable parameters under our approach is only 10% of that of the diffusion models used in (Ghalebikesabi et al., 2023) and achieves a better privacy-accuracy trade-off. Our choice – fine-tune the attention modules only – is inspired by recent observations that altering attention modules in large language models (LLMs) substantially alters the models’ behaviors (Shi et al., 2023; Hu et al., 2021). Therefore, either manipulating or fine-tuning attention modules can yield a more targeted generation, e.g., targeted for a user-preference (Zhang et al., 2023b) and transferring to a target

---

<sup>\*</sup>Equal contribution <sup>1</sup>Department of Computer Science, University of British Columbia, Vancouver, Canada <sup>2</sup>Max Planck Institute for Intelligent Systems, Tuebingen, Germany <sup>3</sup>University of Tübingen, Germany <sup>4</sup>Technical University of Denmark, Denmark. Correspondence to: Saiyue Lyu <saiyuel@cs.ubc.ca>, Michael F. Liu <mflu@cs.ubc.ca>, Margarita Vinaroz <margarita.vinaroz@tuebingen.mpg.de>, Mijung Park <mijungp@cs.ubc.ca>.

distribution (You & Zhao, 2023). See Sec. 3 for further discussion.

The combination of considering LDMs and fine-tuning attention modules using DP-SGD is simple, yet a solid tool whose potential impact is substantial for the following reasons:

- We improve the state-of-the-art (SOTA) results in all three commonly used image benchmark datasets in DP literature, including CIFAR10, CelebA64, and MNIST. This is thanks to the unique aspects of our proposed method, i.e., training DMs in the latent space and fine-tuning only a few selected parameters. This makes our training process considerably more efficient than training a DM from scratch with DP-SGD in (Dockhorn et al., 2023), or fine-tuning the entire DM with DP-SGD in (Ghalebikesabi et al., 2023). Reducing the fine-tuning space not only improves the performance but also helps democratize DP image generation using DMs, which otherwise have to rely on massive computational resources only available to a small fraction of the field and would leave a huge carbon footprint (e.g., reducing the training time from 192 GPU hours (Dockhorn et al., 2023) to mere 10 GPU hours for similar performance).
- We push the boundary of what DP-SGD fine-tuned generative models can achieve, by being the first to produce high-dimensional images (256x256) at a reasonable privacy level. We showcase this in text-conditioned and class-conditioned image generation, where we input a certain text prompt (or a class label) and generate a corresponding image from a DP-fine-tuned LDM for CelebAHQ. These conditional, high-dimensional image generation tasks present more complex but also more realistic benchmarks compared to the conventional CIFAR10 and MNIST datasets. These latter datasets, though widely used in DP image generation literature for years, are now rather simplistic and outdated. Our work contributes to narrowing down the large gap between the current state of synthetic image generation in non-DP settings and that in DP settings.
- We apply the low-rank approximation (Hu et al., 2021) to the attention modules in DMs to further decrease the number of parameters to fine-tune. Interestingly, the performance from LoRA was slightly worse than that of fine-tuning entire attention modules. This is because the large batch size we use improves the signal-to-noise ratio, which significantly helps improve the performance of the full-parameter fine-tuned model, similar to the phenomenon observed in fine-tuning LLMs in Li et al. (2022).

In the following section, we provide relevant background

information. We then present our method along with related work and experiments on benchmark datasets.

## 2. Background

We first describe latent diffusion models (LDMs), then the definition of differential privacy (DP) and finally the DP-SGD algorithm, which we will use to train the LDM in our method.

### 2.1. Latent Diffusion Models (LDMs)

Diffusion Models gradually denoise a normally distributed variable through learning the reverse direction of a Markov Chain of length  $T$ . Latent diffusion models (LDMs) by Rombach et al. (2022) are a modification of denoising diffusion probabilistic models (DDPMs) by Ho et al. (2020) in the following way. First, Rombach et al. (2022) uses a powerful auto-encoder, consisting of an encoder Enc and a decoder Dec. The encoder transforms a high-dimensional pixel representation  $\mathbf{x}$  into a lower-dimensional latent representation  $\mathbf{z}$  via  $\mathbf{z} = \text{Enc}(\mathbf{x})$ ; and the decoder transforms the lower-dimensional latent representation back to the original space via  $\hat{\mathbf{x}} = \text{Dec}(\mathbf{z})$ . Rombach et al. (2022) use a combination of a perceptual loss and a patch-based adversarial objective, with extra regularization for better-controlled variance in the learned latent space, to obtain powerful autoencoders (See section 3 in (Rombach et al., 2022) for details). This training loss encourages the latent representations to carry equivalent information (e.g., the spatial structure of pixels) as the pixel representations, although the dimensionality of the former is greatly reduced.

Second, equipped with the powerful auto-encoder, Rombach et al. (2022) trains a diffusion model (typically a UNet (Ronneberger et al., 2015)) in the latent space. Training a DM in this space can significantly expedite the training process of diffusion models, e.g., from hundreds of GPU days to several GPU hours for similar accuracy.

Third, LDMs also contain attention modules (Vaswani et al., 2017) that take inputs from a conditioning embedder, inserted into the layers of the underlying UNet backbone as the way illustrated in Fig. 1 to achieve flexible conditional image generation (e.g., generating images conditioning on text, image layout, class labels, etc.). The modified Unet is then used as a function approximator  $\tau_{\theta}$  to predict an initial noise from the noisy lower-dimensional latent representations at several finite time steps  $t$ , where in LDMs, the noisy representations (rather than data) follow the diffusion process defined in Ho et al. (2020).

The parameters of the approximator are denoted by  $\theta = [\theta^U, \theta^{Attn}, \theta^{Cn}]$ , where  $\theta^U$  are the parameters of the underlying Unet backbone,  $\theta^{Attn}$  are the parameters of the attention modules, and  $\theta^{Cn}$  are the parameters of the condi-

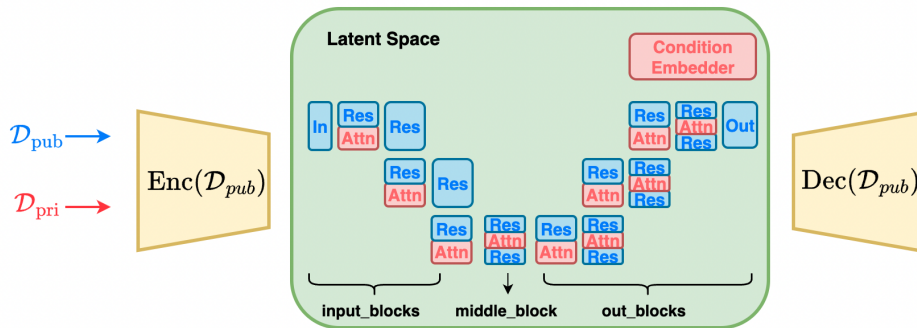


Figure 1: A schematic of DP-LDM. In the non-private step, we pre-train the auto-encoder depicted in yellow (Right and Left) with public data. We then forward pass the public data through the encoder (blue arrow on the left) to obtain latent representations. We then train the diffusion model (depicted in the green box) on the lower-dimensional latent representations. The diffusion model consists of the Unet backbone and added attention modules (in Red) with a conditioning embedder (in Red, at top-right corner). In the private step, we forward pass the private data (red arrow on the left) through the encoder to obtain latent representations of the private data. We then fine-tune only the red blocks, which are attention modules and conditioning embedder, with DP-SGD. Once the training is done, we sample the latent representations from the diffusion model, and pass them through the decoder to obtain the image samples in the pixel space.

tioning embedder (We will explain these further in Sec. 3). These parameters are then optimized by minimizing the prediction error defined by

$$\mathcal{L}_{ldm}(\theta) = \mathbb{E}_{(\mathbf{z}_t, y), \tau, t} [\|\tau - \tau_{\theta}(\mathbf{z}_t, t, y)\|_2^2], \quad (1)$$

where  $\tau \sim \mathcal{N}(0, I)$ ,  $t$  uniformly sampled from  $\{1, \dots, T\}$ ,  $x_t$  is the noisy version of the input  $x$  at step  $t$ ,  $\mathbf{z}_t = \text{Enc}(\mathbf{x}_t)$  and  $y$  is what the model is conditioning on to generate data, e.g., class labels, or a prompt. Once the approximator is trained, the drawn samples in latent space,  $\tilde{\mathbf{z}}$ , are transformed back to pixel space through the decoder, i.e.,  $\tilde{\mathbf{x}} = \text{Dec}(\tilde{\mathbf{z}})$ . Our work introduced in Sec. 3 pre-trains both auto-encoder and  $\tau_{\theta}$  using public data, then fine-tunes only  $\theta_{\text{Attn}}$ ,  $\theta_{\text{Cn}}$ , the parameters of the attention modules and the conditioning embedder, using DP-SGD for private data.

## 2.2. Differential Privacy (DP)

A mechanism  $\mathcal{M}$  is  $(\epsilon, \delta)$ -DP for a given  $\epsilon \geq 0$  and  $\delta \geq 0$  if and only if  $\Pr[\mathcal{M}(\mathcal{D}) \in S] \leq e^{\epsilon} \cdot \Pr[\mathcal{M}(\mathcal{D}') \in S] + \delta$  for all possible sets of the mechanism’s outputs  $S$  and all neighbouring datasets  $\mathcal{D}, \mathcal{D}'$  that differ by a single entry. A single entry difference could come from either replacing or including/excluding one entry to/from the dataset  $\mathcal{D}$ .

One of the most well-known and widely used DP mechanisms is the *Gaussian mechanism*. The Gaussian mechanism adds a calibrated level of noise to a function  $\mu : \mathcal{D} \mapsto \mathbb{R}^p$  to ensure that the output of the mechanism is  $(\epsilon, \delta)$ -DP:  $\tilde{\mu}(\mathcal{D}) = \mu(\mathcal{D}) + n$ , where  $n \sim \mathcal{N}(0, \sigma^2 \Delta_{\mu}^2 \mathbf{I}_p)$ . Here,  $\sigma$  is often called a privacy parameter, which is a function of  $\epsilon$  and  $\delta$ .  $\Delta_{\mu}$  is often called the *global sensitivity* (Dwork et al., 2006; 2014), which is the maximum difference in  $L_2$ -norm given two neighbouring  $\mathcal{D}$  and  $\mathcal{D}'$ ,  $\|\mu(\mathcal{D}) - \mu(\mathcal{D}')\|_2$ .

Because we are adding noise, the natural consequence is that the released function  $\tilde{\mu}(\mathcal{D})$  is less accurate than the non-DP counterpart,  $\mu(\mathcal{D})$ . This introduces privacy-accuracy trade-offs.

DP-SGD (Abadi et al., 2016) is an instantiation of the Gaussian mechanism in stochastic gradient descent (SGD) by adding an appropriate amount of Gaussian noise to the gradients in every training step, to ensure the parameters of a neural network are differentially private. When using DP-SGD, due to the composability property of DP (Dwork et al., 2006; 2014), privacy loss is accumulating over a typically long course of training. Abadi et al. (2016) exploit the subsampled Gaussian mechanism (i.e., applying the Gaussian mechanism on randomly subsampled data) to achieve a tight privacy bound. The *Opacus* package (Yousefpour et al., 2021) implements the privacy analysis in DP-SGD, which we adopt in our method. One thing to note is that we use the **inclusion/exclusion** definition of DP in the experiments as in *Opacus*.

## 3. Differentially private latent diffusion models (DP-LDMs)

In our method, which we call *differentially private latent diffusion models (DP-LDMs)*, we carry out two training steps: non-private and private steps.

**Non-Private Step: Pre-training an autoencoder and a DM using public data.** Following Rombach et al. (2022), we first pre-train an auto-encoder. The encoder scales down an image  $\mathbf{x} \in \mathbb{R}^{H \times W \times 3}$  to a 3-dimensional latent representation  $\mathbf{z} \in \mathbb{R}^{h \times w \times c}$  by a factor of  $f$ , where

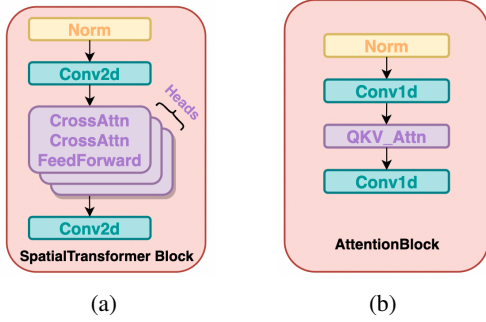


Figure 2: (a) is a SpatialTransformer Block; (b) is an AttentionBlock

$f = H/h = W/w$ . This 3-dimensional latent representation is chosen to take advantage of image-specific inductive biases that the Unet contains, e.g., 2D convolutional layers. Following Rombach et al. (2022), we also train the autoencoder by minimizing a combination of different losses, such as perceptual loss and adversarial loss, with some form of regularization. See Appendix Sec. A.1 for details. As noted by Rombach et al. (2022), we also observe that a mild form of downsampling performs the best, achieving a good balance between training efficiency and perceptually decent results. See Appendix Sec. A.1 for details on different scaling factors  $f = 2^m$ , with a different value of  $m$ . Training an auto-encoder does not incur any privacy loss, as we use public data  $\mathcal{D}_{pub}$  that is similar to private data  $\mathcal{D}_{priv}$  at hand. The trained autoencoder is, therefore, a function of public data: an encoder  $\text{Enc}(\mathcal{D}_{pub})$  and a decoder  $\text{Dec}(\mathcal{D}_{pub})$ .

A forward pass through the trained encoder  $\text{Enc}(\mathcal{D}_{pub})$  gives us a latent representation of each image, which we use to train a diffusion model. As in (Rombach et al., 2022), we consider a modified Unet for the function approximator  $\tau_\theta$  shown in Fig. 1. We minimize the loss given in (1) to estimate the parameters of  $\tau_\theta$  as:

$$\theta_{\mathcal{D}_{pub}}^U, \theta_{\mathcal{D}_{pub}}^{Attn}, \theta_{\mathcal{D}_{pub}}^{Cn} = \arg \min_{\theta} \mathcal{L}_{ldm}(\theta). \quad (2)$$

Since we use public data, there is no privacy loss incurred in estimating the parameters, which are a function of public data  $\mathcal{D}_{pub}$ .

**Private Step: Fine-tuning attention modules & conditioning embedder for private data.** Given a pre-trained diffusion model, we fine-tune the attention modules and a conditioning embedder using our private data.

For the models with the conditioned generation, the attention modules refer to the spatial transformer blocks shown in Fig. 2(a) which contains cross-attentions and multiple heads. For the models with an unconditional generation, the attention modules refer to the attention blocks shown in Fig. 2(b). Consequently, the parameters of the attention

modules, denoted by  $\theta^{Attn}$ , differ, depending on the conditioned or unconditioned cases. The conditioning embedder only exists in the conditioned case. Depending on the different modalities the model is trained on, the conditioning embedder takes a different form. For instance, if the model generates images conditioning on the class labels, the conditioning embedder is simply a class embedder, which embeds class labels to a latent dimension. If the model conditions on language prompts, the embedder can be a transformer.

The core part of the spatial transformer block and the attention block is the attention layer, which has the following parameterization (For simplicity, we explain it under the conditioned case):

$$\begin{aligned} & \text{Attention}(\psi_i(\mathbf{z}_t), \phi(y); Q, K, V) \\ &= \text{softmax}\left(\frac{QK^T}{\sqrt{d_k}}\right)V \in \mathbb{R}^{N \times d_k}, \end{aligned} \quad (3)$$

where  $\psi_i(\mathbf{z}_t) \in \mathbb{R}^{N \times d^i}$  is an intermediate representation of the latent representation  $\mathbf{z}_t$  through the  $i$ th residual convolutional block in the backbone Unet, and  $\phi(y) \in \mathbb{R}^{M \times d_c}$  is the embedding of what the generation is conditioned on (e.g., class labels, or CLIP embedding). Furthermore,  $Q = \psi_i(\mathbf{z}_t)W_Q^{(i)\top}$ ,  $K = \phi(y)W_K^{(i)\top}$ , and  $V = \phi(y)W_V^{(i)\top}$ , where the parameters are denoted by  $W_Q^{(i)} \in \mathbb{R}^{d_k \times d^i}$ ;  $W_K^{(i)} \in \mathbb{R}^{d_k \times d_c}$ ; and  $W_V^{(i)} \in \mathbb{R}^{d_k \times d_c}$ . Unlike the conditioned case, where the key ( $K$ ) and value ( $V$ ) vectors are computed as a projection of the conditioning embedder, the key and value vectors are a projection of the pixel embedding  $\psi_i(\mathbf{z}_t)$  only in the case of the unconditioned model. We run DP-SGD to fine-tune these parameters to obtain differentially private  $\theta_{\mathcal{D}_{priv}}^{Attn}$  and  $\theta_{\mathcal{D}_{priv}}^{Cn}$ , starting from  $\theta_{\mathcal{D}_{pub}}^{Attn}, \theta_{\mathcal{D}_{pub}}^{Cn}$ . Our algorithm is given in Algorithm 1.

**Why fine-tune attention modules?** Our rationale behind this choice is as follows. The output of the attention in (3) assigns a high focus to the features that are more important, by zooming into what truly matters in an image depending on a particular context, e.g., relevant to what the image is conditioned on. This can be quite different when we move from one distribution to the other. By fine-tuning the attention modules (together with the conditioning embedder when conditioned case), we are able to effectively transfer what we learned from the public data distribution to the private data distribution, as shown in Sec. 5. However, if we fine-tune other parts of the model, e.g., the ResBlocks, the fine-tuning of these blocks can make a large change in the features themselves, which can significantly reduce the performance in the private training (See Sec. 5).

The idea of fine-tuning attention blocks is explored elsewhere. For instance, in fine-tuning large language models, existing work introduces a few new parameters to transformer attention blocks, and those new parameters are fine-

**Algorithm 1** DP-LDM

**Input:** Latent representations through a pre-trained auto-encoder and conditions (if conditioned generation)  $\{(\mathbf{z}_i, y_i)\}_{i=1}^N$ , a pre-trained diffusion model with parameters  $\theta$ , number of iterations  $P$ , mini-batch size  $B$ , clipping norm  $C$ , learning rate  $\eta$ , privacy parameter  $\sigma$  corresponding to  $(\epsilon, \delta)$ -DP. Denote  $\hat{\theta} = \{\theta^{Attn}, \theta^{Cn}\}$

**for**  $p = 1$  **to**  $P$  **do**

**Step 1.** Take a mini-batch  $B_p$  uniformly at random with a sampling probability,  $q = B/N$

**Step 2.** For each sample  $i \in B_p$  compute the gradient:

$$g_p(\mathbf{z}_i, y_i) = \nabla_{\hat{\theta}_p} \mathcal{L}_{ldm}(\hat{\theta}_p, \mathbf{z}_i, y_i)$$

**Step 3.** Clip the gradient:

$$\hat{g}_p(\mathbf{z}_i, y_i) = g_p(\mathbf{z}_i, y_i) / \max(1, \|g_p(\mathbf{z}_i, y_i)\|_2 / C)$$

**Step 4.** Add noise:

$$\tilde{g}_p = \frac{1}{B} \left( \sum_{i=1}^B \hat{g}_p(\mathbf{z}_i, y_i) + \mathcal{N}(0, \sigma^2 C^2 I) \right)$$

**Step 5.** Gradient descent:  $\hat{\theta}_{p+1} = \hat{\theta}_p - \eta \tilde{g}_p$

**end for**

**Return:**  $(\epsilon, \delta)$ -differentially private  $\hat{\theta}_P = \{\theta_P^{Attn}, \theta_P^{Cn}\}$

tuned (Yu et al., 2022; Hu et al., 2021) to adapt to new distributions. In the context of pre-trained diffusion models, adding, modifying, and controlling attention layers are gaining popularity for tasks such as image editing and text-to-image generation (Hertz et al., 2022; Park et al., 2023; Zhang et al., 2023a; You & Zhao, 2023).

**Which public dataset to use given a private dataset?**

This is an open question in transfer learning literature. Generally, if the two datasets are close to each other in *some* sense, they are assumed to be a better pair. However, similarity *in what sense* has to be chosen differently depending on a particular data domain and appropriately privatized if private data is used in this step. We believe using FID as a proxy to judge the similarity between two *image* datasets is sensible (See Sec. 5.1 how we privatize this step). In other datasets, out of the image domain, there could be a more appropriate metric to use than FID, e.g., in the case of discrete data, kernel-based distance metrics with an appropriately chosen kernel could be more useful.

## 4. Related Work

Early efforts in differentially private data generation imposes strict limitations on the data type and the intended purpose of the released data (Snok & Slavković, 2018; Mohammed et al., 2011; Xiao et al., 2010; Hardt et al., 2012; Zhu et al., 2017), which leads to the difficulties in generating large-scale data. Later, several works have explored generating discrete data with restricted range of values, by understanding the relationships of small groups of features and then privatizing them (Zhang et al., 2017; Qardaji et al.,

2014; Chen et al., 2015; Zhang et al., 2021). However, these techniques cannot be applied to high-dimensional data due to the constraint of discretization. Recently, more efforts have focused on leveraging advanced generative models to achieve better differentially private synthetic data (Hu et al., 2023). Some of them (Xie et al., 2018; Torkzadehmani et al., 2019; Frigerio et al., 2019; Yoon et al., 2019; Chen et al., 2020) utilize generative adversarial networks (GANS) (Goodfellow et al., 2014), or trained GANs with the PATE structure (Papernot et al., 2017). Other works have employed variational autoencoders (VAEs) (Acs et al., 2018; Jiang et al., 2022; Pfizner & Arnrich, 2022), or proposed customized structures (Harder et al., 2021; Vinaroz et al., 2022; Cao et al., 2021; Liew et al., 2022a; Harder et al., 2023). For instance, Harder et al. (2023) pretrained perceptual features using public data and privatized only data-dependent terms using maximum mean discrepancy.

Limited works have so far delved into privatizing diffusion models. Dockhorn et al. (2023) develop a DP score-based generative models (Song et al., 2021) using DP-SGD, applied to relatively simple datasets such as MNIST, FashionMNIST and CelebA (downsampled to  $32 \times 32$ ). Ghalebikesabi et al. (2023) fine-tune the ImageNet pre-trained diffusion model (DDPM) (Ho et al., 2020) with more than 80 M parameters using DP-SGD for CIFAR-10. We instead adopt a different model (LDM) and fine-tune only the small part of the DM in our model to achieve better privacy-accuracy trade-offs. As concurrent work to ours, Lin et al. (2023) propose a DP-histogram mechanism to generate synthetic data through the utilization of publicly accessible APIs. Due to their reliance on APIs, the resolution of generated synthetic image to represent private data is determined by the resolution of the APIs’ outputs. Additionally, the effectiveness of the method is more heavily influenced by the similarity between the private data and the data used to train the APIs, than methods involve training and fine-tuning. Since Lin et al. (2023) explores a different context, i.e., not training or fine-tuning diffusion models, we refrain from directly comparing our method to theirs.

## 5. Experiments

We demonstrate the performance of our method in comparison with the state-of-the-art methods in DP data generation, using several combinations of public/private data of different levels of complexity at varying privacy levels.

**Implementation.** We implemented DP-LDMs in PyTorch Lightning (Paszke et al., 2019) building on the LDM codebase by Rombach et al. (2022) and Opacus (Yousefpour et al., 2021) for DP-SGD training. Several recent papers present the importance of using large batches in DP-SGD training to improve accuracy at a fixed privacy level (Ponomareva et al., 2023; De et al., 2022; Bu et al., 2022). To

Table 1: Private and public dataset pairs, with corresponding evaluation metric and choices of classifiers.

Private Dataset	Public Dataset	Similarity Evaluation	Downstream Classifiers
MNIST (LeCun & Cortes, 2010)	EMNIST(letter) (Cohen et al., 2017)	-	CNN, WRN40-4
CIFAR-10 (Krizhevsky et al., 2009)	ImageNet32 (Deng et al., 2009)	FID	ResNet-9, WRN40-4
Camelyon17-WILDS (Koh et al., 2021)	ImageNet32 (Deng et al., 2009)	-	WRN40-4
CelebA32 (Liu et al., 2015)	ImageNet32 (Deng et al., 2009)	FID	-
CelebA64 (Liu et al., 2015)	ImageNet64 (Deng et al., 2009)	FID	ResNet-9
CelebAHQ (Karras et al., 2018)	ImageNet256 (Deng et al., 2009)	FID	-
MM-CelebAHQ (Xia et al., 2021)	LAION-400M (Schuhmann et al., 2021)	FID	-

incorporate this finding in our work, we wrote custom batch splitting code that integrates with Opacus and Pytorch Lightning, allowing us to test arbitrary batch sizes. Our DP-LDM also improves significantly with large batches as will be shown soon, consistent with the findings in recent work. For our experiments incorporating LoRA, we use the loralib (Hu et al., 2021) Python library.

**Datasets<sup>1</sup> and Evaluation.** We list all the private and public dataset pairs with corresponding evaluation metrics in Table 1. Regarding high-quality generation, we use CelebAHQ for class conditional generation and Multi-Modal-CelebAHQ (MM-CelebAHQ) for text-to-image generation. Our choice of evaluation metric is either based on standard practice or following previous work to do a fair comparison. We measure the model performance by computing the Fréchet Inception Distance (FID) (Heusel et al., 2017) between the generated samples and the real data. For downstream task, we consider CNN (LeCun et al., 2015), ResNet-9 (He et al., 2016), and WRN40-4 (Zagoruyko & Komodakis, 2017) to evaluate the classification performance of synthetic data. Each number in our tables represents an average value across three independent runs, with a standard deviation (unless stated otherwise). Note that some standard deviation values are reported as 0.0 due to rounding. Values for comparison methods are taken from their papers, with an exception for the DP-MEPF comparison to CelebAHQ, which we ran their code by loading this data.

### 5.1. Comparisons to State-of-the-art methods

We start with testing our method on private and public dataset pairs at varying complexity, which are generally considered to be relatively similar to each other. In particular, we present the results of transferring from Imagenet to CIFAR-10 and CelebA distributions and from EMNIST to

<sup>1</sup>Dataset licenses: MNIST: CC BY-SA 3.0; CelebA: see <https://mmlab.ie.cuhk.edu.hk/projects/CelebA.html>; CIFAR-10: MIT; Camelyon17: CC0

		$\epsilon = 10$	$\epsilon = 5$	$\epsilon = 1$
CIFAR-10 32x32 ( $\delta = 10^{-5}$ )	<b>DP-LDM(ours)</b>	<b>8.4 ± 0.2</b>	<b>13.4 ± 0.4</b>	<b>22.9 ± 0.5</b>
	DP-Diffusion	9.8	15.1	25.2
	DP-MEPF ( $\phi_1, \phi_2$ )	29.1	30.0	54.0
	DP-MEPF ( $\phi_1$ )	30.3	35.6	56.5
	DPDM	97.7	-	-
CelebA 32x32 ( $\delta = 10^{-6}$ )	<b>DP-LDM(ours)</b>	<b>16.2 ± 0.2</b>	<b>16.8 ± 0.3</b>	<b>25.8 ± 0.9</b>
	DP-MEPF ( $\phi_1$ )	16.3	17.2	<b>17.2</b>
	DP-GAN (pre-trained)	58.1	66.9	81.3
	DPDM	21.2	-	71.8
	DP Sinkhorn	189.5	-	-
CelebA 64x64 ( $\delta = 10^{-6}$ )	<b>DP-LDM(ours)</b>	<b>14.3 ± 0.1</b>	<b>16.1 ± 0.2</b>	<b>21.1 ± 0.2</b>
	DP-MEPF ( $\phi_1$ )	17.4	16.5	<b>20.4</b>
	DP-GAN (pre-trained)	57.1	62.3	72.5
	DPDM	78.3	-	-

Table 2: FID scores (lower is better) for synthetic CIFAR-10, CelebA32, and CelebA64 data, in comparison with DP-Diffusion (Ghalebikesabi et al., 2023), DP-MEPF (Harder et al., 2023), DPDM (Dockhorn et al., 2023), DP-GAN (Xie et al., 2018), and DP Sinkhorn (Cao et al., 2021).

MNIST distribution. Additionally, to test our method’s effectiveness at transferring knowledge across a large domain gap, we present the results of transferring from Imagenet to Camelyon17-WILDS. Further details on these experiments are available in appendix A.

**FID.** Comparison to other SOTA methods in terms of FID (the lower the better) is illustrated in Table 2. When tested on CIFAR-10, our DP-LDM outperforms other methods at all epsilon levels ( $\epsilon = 1, 5, 10$  and  $\delta = 10^{-5}$ ). These FID values correspond to the case where only 9-16 attention modules are fine-tuned (i.e., fine-tuning only 10% of trainable parameters in the model) and the rest remain fixed. See Table 11 for ablation experiments for fine-tuning different attention modules.

When tested on CelebA32 and CelebA64, our unconditional LDM achieves new SOTA results at  $\epsilon = 10, 5$  and are comparable to DP-MEPF at  $\epsilon = 1$ . Samples are available in Figure 8.

**Downstream Classification.** FID can be viewed as a fidelity metric, serving as a proxy for the utility of the synthetic data. To directly present the utility results of the model, we also consider accuracy on the classification task, which is listed in Table 3. All the classifiers are trained with 50K synthetic samples and then evaluated on real data samples. For each dataset, we follow previous work to choose classifier models for a fair comparison.

When tested on CIFAR-10, DP-LDM outperforms others at all epsilon levels. For testing on CelebA64, we began with an LDM pre-trained on conditional ImageNet at the same resolution, and then fine-tuned it on CelebA where the (binary) class labels were given by the “Male” attribute. Our method achieves a new SOTA performance at all epsilon levels.

**DP-LDMs: Differentially Private Latent Diffusion Models**

		$\epsilon = 10$	$\epsilon = 5$	$\epsilon = 1$
CIFAR-10 ResNet-9	<b>DP-LDM(ours)</b>	<b>65.3 ± 0.3</b>	<b>59.1 ± 0.2</b>	<b>51.3 ± 0.1</b>
	DP-MEPF ( $\phi_1, \phi_2$ )	48.9	47.9	28.9
	DP-MEPF ( $\phi_1$ )	51.0	48.5	29.4
	DP-MERF	13.2	13.4	13.8
CIFAR-10 WRN40-4	<b>DP-LDM(ours)</b>	<b>78.6 ± 0.3</b>	-	-
	DP-Diffusion	75.6	-	-
CelebA64 ResNet-9	<b>DP-LDM(ours)</b>	<b>96.4 ± 0.0</b>	<b>96.0 ± 0.0</b>	<b>94.5 ± 0.0</b>
	DP-MEPF ( $\phi_1$ )	93.9 ± 2.1	93.7	82.9
MNIST CNN	<b>DP-LDM(ours)</b>	97.4 ± 0.1	<b>96.8</b>	<b>95.9 ± 0.1</b>
	DPDM	<b>98.1</b>	-	95.2
MNIST WRN-40-4	<b>DP-LDM(ours)</b>	97.5 ± 0.0	-	-
	DP-Diffusion	<b>98.6</b>	-	-
Camelyon17- WILDS WRN-40-4	<b>DP-LDM(ours)</b>	85.4 ± 0.0	-	-
	DP-Diffusion	<b>91.1</b>	-	-

Table 3: Test accuracies (higher is better) for synthetic CIFAR-10, CelebA64, and MNIST data, in comparison with DP-MEPF (Harder et al., 2023), DP-MERF (Harder et al., 2021), DP-Diffusion (Ghalebikesabi et al., 2023), and DPDM (Dockhorn et al., 2023). The choices of classifier architecture is given under each dataset name.

When tested on MNIST, we beat the previous methods at  $\epsilon = 1$  and achieve comparable results at  $\epsilon = 10$ . One thing to note is that DPDM takes 1.75M parameters and 192 GPU hours to achieve 98.1 accuracy, and DP-Diffusion takes 4.2M parameters (GPU hours not showing), while our methods takes only 0.8M parameters and 10 GPU hours to achieve 97.4 accuracy, which significantly reduces the parameters and saves much computing resources.

When tested on Camelyon17, our method slightly underperforms than Ghalebikesabi et al. (2023), possibly due to their use of a pre-trained WRN-40-4 classifier (pre-trained with ImageNet32), as opposed to our training of the classifier from scratch.

**Why do we select EMNIST as a public dataset?** Previous work (Harder et al., 2023) used SVHN as a public dataset to MNIST since they are both number images. However, SVHN and MNIST differ significantly (SVHN contains several digits per image with 3 channels while MNIST contains one digit per image with 1 channel). So we considered other, more similar datasets such as EMNIST and KMNIST as public dataset candidates. Here, we use FID scores to judge the closeness between public and private data. Since we use a private dataset for this selection, we privatize the FID statistics following the mechanisms used in (Park et al., 2017) to compute the FID score in a DP manner. Based on the results, we chose EMNIST. In addition, we also did ablation experiments of SVHN and KMNIST as shown in Table 9, which verifies our choice of EMNIST. More details can be found in Appendix Sec. A.2.

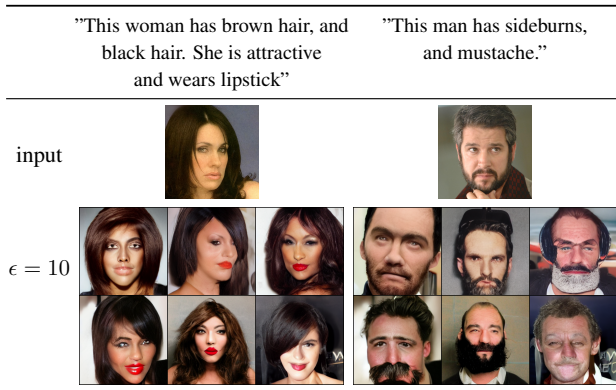


Figure 3: Text-to-image generation for CelebAHQ 256 by 256 with prompt inputs under  $\epsilon = 10$ . We achieve an FID of 15.6 at  $\epsilon = 10$ .

### 5.2. Differentially private high-quality image generation

With the latent representations of the inputs, LDMs can better improve DP training. To the best of our knowledge, we are the first to achieve high-dimensional differentially private generation.

**Text-to-image generation.** For text-to-image generation, we fine-tune the LDM models pretrained with LAION-400M (Schuhmann et al., 2021) for MM-CelebAHQ ( $256 \times 256$ ). Each image is described by a caption, which is fed to the conditioning embedder, BERT (Devlin et al., 2018). We freeze the BERT embedder as well during fine-tuning attention modules to reduce the trainable parameters, then we bring back BERT for sampling. DP-LDM achieves FID scores of 15.6 for  $\epsilon = 10$ . As illustrated in Fig. 5.2, the samples are faithful to our input prompts, but not identical to the training sample, unlike the memorization behavior of the non-private Stable Diffusion (Carlini et al., 2023).

**Class conditional generation.** We build our model on the LDM model provided by Rombach et al. (2022) which is pretrained on Imagenet at a resolution of  $256 \times 256$ . Following our experiments in Section 5.1, we fine-tune all of the SpatialTransformer blocks. While CelebAHQ does not provide class labels, each image is associated with 40 binary attributes. We choose the attribute “Male” to act as a binary class label for each image. Generated samples are available in Figure 5.2 along with FID values. Compared to DP-MEPF, based on the FID scores and perceptual image quality, DP-LDM is better suited for generating detailed, plausible samples from the high-resolution dataset at a wide range of privacy levels.

### 5.3. Ablation studies

In this section, we present ablation studies for strategically improving performances and reducing parameters.

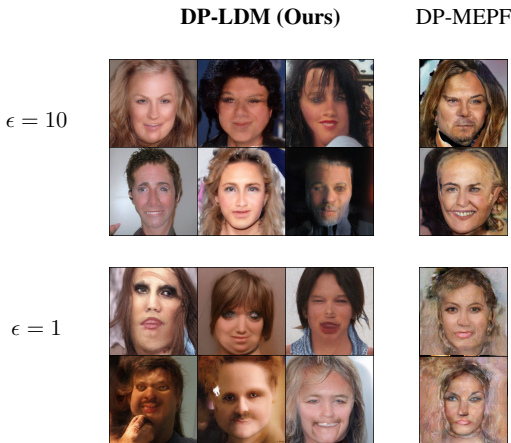


Figure 4: Synthetic  $256 \times 256$  CelebA samples generated at different levels of privacy. Samples for DP-MEPF are generated from code available in [Harder et al. \(2023\)](#). We computed FID between our generated samples and the real data and achieve FIDs of  $19.0 \pm 0.0$  at  $\epsilon = 10$ ,  $20.5 \pm 0.1$  at  $\epsilon = 5$ , and  $25.6 \pm 0.1$  at  $\epsilon = 1$ . DP-MEPF achieves an FID of 41.8 at  $\epsilon = 10$  and 101.5 at  $\epsilon = 1$ .

Table 4: **Top.** Effect of increasing batch size on FID (CelebA64). At a fixed epsilon level, larger batches improve FIDs. **Bottom.** Effect of fine-tuning only the selected part of the model (CIFAR-10). At a fixed epsilon level, fine-tuning attention modules only achieves best results.

		$\epsilon = 10$	$\epsilon = 5$	$\epsilon = 1$
Batch Size	<b>8192</b>	<b><math>14.3 \pm 0.1</math></b>	<b><math>16.1 \pm 0.2</math></b>	<b><math>21.1 \pm 0.2</math></b>
	2048	$16.2 \pm 0.2$	$17.1 \pm 0.2$	$22.1 \pm 0.1$
	512	$17.2 \pm 0.1$	$18.0 \pm 0.1$	$22.3 \pm 0.2$
Fine-tune Different Parts	<b>Attention Modules</b>	<b><math>8.4 \pm 0.2</math></b>	<b><math>13.4 \pm 0.4</math></b>	<b><math>22.9 \pm 0.5</math></b>
	Resblocks	105.5	127.7	149.7
	Out_blocks	45.8	48.3	57.2
	Input_blocks	54.2	56.9	70.4

**Increasing batch size.** Table 4 (Top) shows results for DP-LDM trained with CelebA64 under different training batch sizes, which provides evidence suggesting that training with larger batch sizes improves the performance of the model.

**Fine-tuning attention modules at different layers.** To further reduce more trainable parameters, we consider fine-tuning only a portion of attention modules See Table 11 for CIFAR-10 and Table 10 for MNIST. See also Appendix Sec. A.3 and Appendix Sec. A.2.3 for details. The best results are achieved when fine-tuning the attention modules in the out\_blocks in the Unet (out\_blocks shown in Fig. 1), consistently throughout all datasets we tested. Based on this observation, here is general guidance on fine-tuning strategy: if a limited privacy budget is given, we suggest fine-tuning the attention modules in the out\_blocks only to achieve better accuracies.

Table 5: FID scores (lower is better) for incorporating LoRA into DP-LDM with different ranks with CelebA64 (trained for 50 epochs).

Rank	DP-LDM	LoRA (differ in rank)				
		64	8	4	2	1
$\epsilon = 10$	<b>15.2</b>	17.4	18.1	19.0	19.9	22.0
$\epsilon = 5$	<b>16.2</b>	18.9	18.3	20.4	22.0	22.6
$\epsilon = 1$	<b>21.7</b>	25.5	23.0	23.8	25.0	25.8
# Parameters	8.0M	1.3M	16k	80k	40k	20k
trainable/total	11.03%	1.74%	0.22%	0.11%	0.06%	0.03%

**Fine-tuning a different part of the Unet.** Previous results focused on fine-tuning attention modules at varying layers. Here, we present the performance of fine-tuning a different part of the Unet while the rest of the model is frozen. In Table 4 (Bottom), we show the FID scores evaluated on synthetic CIFAR10 images. The main takeaway messages are (a) fine-tuning Resblocks hurts the performance, possibly because the learned features during the pre-training stage are altered, and (b) fine-tuning out\_blocks is more useful than input\_blocks, while the best strategy is fine-tuning the attention modules in the out\_blocks.

**Applying LoRA to DP-LDM.** To reduce the fine-tuning parameters, previous work (Yu et al., 2022) has explored LoRA during training. We performed additional experiments by applying LoRA to the QKV matrices in all the attention modules. As shown in Table 5, LoRA was not particularly useful and our current DP-LDM still outperformed. This might surprise readers. However, this phenomenon was previously observed in fine-tuning LLMs (Li et al., 2022). They reasoned that the large batch size improves the signal-to-noise ratio (shown in Fig 3 [1] of Li et al. (2022)), which significantly helps improve the performance of the model with full updates. We find that this is analogous to our results. When we fine-tune the parameters in the attention modules in their original ranks, we keep the full-rank information, while low-rank approximations generally lose information. Due to the large batch size we use (bs=8192), we maintain a relatively good signal-to-noise ratio in the gradients perturbed by DP-SGD, which leads to better performance than LoRA at the same privacy level. It could be an intriguing direction to pursue whether the intrinsic dimensionality of the gradients is truly low when fine-tuning DP-LDMs, through the metric used in Aghajanyan et al. (2020) to empirically evaluate the intrinsic dimension.

## 6. Conclusion

In *Differentially Private Latent Diffusion Models* (DP-LDM), we utilize DP-SGD to fine-tune only the attention modules (and embedders for conditioned generation) of the pretrained LDM at varying layers with privacy-sensitive data. We demonstrate that our method is capable of gen-



erating quality images in various scenarios. We perform an in-depth analysis of the ablation of DP-LDM to explore the strategy for reducing parameters for more applicable training of DP-SGD. Based on our promising results, we conclude that fine-tuning LDMs is an efficient and effective framework for DP generative learning. We hope our results can contribute to future research in DP data generation, considering the rapid advances in diffusion-based generative modelling.

## Impact Statement

As investigated in (Carlini et al., 2023), diffusion models can memorize individual images from the training data and give the same as generating samples. Aiming to bring positive effects to society, our research is driven by the necessity of robust and scalable data privacy. However, it is also important to approach the use of public data cautiously. As (Tramèr et al., 2022) pointed out, public data themselves may still be sensitive due to a lack of curation practices. In addition, the public data usually achieves similar distribution as the private data, however, no proper public data is available currently as this might require heavy domain shift of the data themselves. We understand these potential issues, but current DP machine learning research leads to minimal effects because of the inadequacy of the utility. From our perspective, auxiliary public data still emerges as the most promising option for attaining satisfactory utility, compared to the potential harm it might inject. We hope our discussion will contribute to further research in differential privacy in machine learning using public data.

To further guarantee the reproducibility, our code is available at <https://anonymous.4open.science/r/DP-LDM-4525> with detailed instructions. And all the hyperparameters are discussed in detail in Appendix Sec. B.

## References

- Abadi, M., Chu, A., Goodfellow, I. J., McMahan, H. B., Mironov, I., Talwar, K., and Zhang, L. Deep learning with differential privacy. In *Proceedings of the 2016 ACM SIGSAC Conference on Computer and Communications Security, CCS '16*, pp. 308–318, New York, NY, USA, 2016. Association for Computing Machinery. ISBN 9781450341394. doi: 10.1145/2976749.2978318.
- Acs, G., Melis, L., Castelluccia, C., and De Cristofaro, E. Differentially private mixture of generative neural networks. *IEEE Transactions on Knowledge and Data Engineering*, 31(6):1109–1121, 2018.
- Aghajanyan, A., Zettlemoyer, L., and Gupta, S. Intrinsic dimensionality explains the effectiveness of language model fine-tuning. In *Proceedings of the 59th Annual Meeting of the Association for Computational Linguistics and the 11th International Joint Conference on Natural Language Processing*, 2020.
- Bie, A., Kamath, G., and Zhang, G. Private GANs, revisited. In *NeurIPS 2022 Workshop on Synthetic Data for Empowering ML Research*, 2022.
- Bu, Z., Mao, J., and Xu, S. Scalable and efficient training of large convolutional neural networks with differential privacy, 2022.
- Cao, T., Bie, A., Vahdat, A., Fidler, S., and Kreis, K. Don’t generate me: Training differentially private generative models with sinkhorn divergence. In *Neural Information Processing Systems (NeurIPS)*, 2021.
- Carlini, N., Hayes, J., Nasr, M., Jagielski, M., Sehwag, V., Tramèr, F., Balle, B., Ippolito, D., and Wallace, E. Extracting training data from diffusion models. In *Proceedings of the 32nd USENIX Conference on Security Symposium, SEC '23, USA*, 2023. USENIX Association. ISBN 978-1-939133-37-3.
- Chen, D., Orekondy, T., and Fritz, M. Gs-wgan: A gradient-sanitized approach for learning differentially private generators. In *Advances in Neural Information Processing Systems 33*, 2020.
- Chen, R., Xiao, Q., Zhang, Y., and Xu, J. Differentially private high-dimensional data publication via sampling-based inference. In *Proceedings of the 21th ACM SIGKDD International Conference on Knowledge Discovery and Data Mining*, pp. 129–138, 2015.
- Cohen, G., Afshar, S., Tapson, J., and Van Schaik, A. Emnist: Extending mnist to handwritten letters. In *2017 international joint conference on neural networks (IJCNN)*, pp. 2921–2926. IEEE, 2017.
- De, S., Berrada, L., Hayes, J., Smith, S. L., and Balle, B. Unlocking high-accuracy differentially private image classification through scale, 2022.
- Deng, J., Dong, W., Socher, R., Li, L.-J., Li, K., and Fei-Fei, L. Imagenet: A large-scale hierarchical image database. In *2009 IEEE conference on computer vision and pattern recognition*, pp. 248–255. Ieee, 2009.
- Devlin, J., Chang, M.-W., Lee, K., and Toutanova, K. Bert: Pre-training of deep bidirectional transformers for language understanding. *arXiv preprint arXiv:1810.04805*, 2018.
- Dockhorn, T., Cao, T., Vahdat, A., and Kreis, K. Differentially private diffusion models, 2023. URL <https://openreview.net/forum?id=pX21pH4CsNB>.

- Duan, J., Kong, F., Wang, S., Shi, X., and Xu, K. Are diffusion models vulnerable to membership inference attacks? In *Proceedings of the 40th International Conference on Machine Learning, ICML'23*. JMLR.org, 2023.
- Dwork, C., Kenthapadi, K., McSherry, F., Mironov, I., and Naor, M. Our data, ourselves: Privacy via distributed noise generation. In *Advances in Cryptology - EUROCRYPT 2006, 25th Annual International Conference on the Theory and Applications of Cryptographic Techniques*, volume 4004 of *Lecture Notes in Computer Science*, pp. 486–503. Springer, 2006. doi: 10.1007/11761679\_29.
- Dwork, C., Roth, A., et al. The algorithmic foundations of differential privacy. *Foundations and Trends® in Theoretical Computer Science*, 9(3–4):211–407, 2014.
- Frigerio, L., de Oliveira, A. S., Gomez, L., and Duverger, P. Differentially private generative adversarial networks for time series, continuous, and discrete open data. In *ICT Systems Security and Privacy Protection - 34th IFIP TC 11 International Conference, SEC 2019, Lisbon, Portugal, June 25-27, 2019, Proceedings*, pp. 151–164, 2019. doi: 10.1007/978-3-030-22312-0\_11.
- Ghalebikesabi, S., Berrada, L., Gowal, S., Ktena, I., Stanforth, R., Hayes, J., De, S., Smith, S. L., Wiles, O., and Balle, B. Differentially private diffusion models generate useful synthetic images, 2023.
- Goodfellow, I. J., Pouget-Abadie, J., Mirza, M., Xu, B., Warde-Farley, D., Ozair, S., Courville, A., and Bengio, Y. Generative adversarial networks. In *Advances in Neural Information Processing Systems*, 2014.
- Harder, F., Adamczewski, K., and Park, M. DP-MERF: Differentially private mean embeddings with random features for practical privacy-preserving data generation. In *AISTATS*, volume 130 of *Proceedings of Machine Learning Research*, pp. 1819–1827. PMLR, 2021.
- Harder, F., Jalali, M., Sutherland, D. J., and Park, M. Pre-trained perceptual features improve differentially private image generation. *Transactions on Machine Learning Research*, 2023. ISSN 2835-8856. URL <https://openreview.net/forum?id=R6W7zkMz0P>.
- Hardt, M., Ligett, K., and Mcsherry, F. A simple and practical algorithm for differentially private data release. In *Advances in Neural Information Processing Systems 25*, pp. 2339–2347. Curran Associates, Inc., 2012.
- He, K., Zhang, X., Ren, S., and Sun, J. Deep residual learning for image recognition. In *Proceedings of the IEEE conference on computer vision and pattern recognition*, pp. 770–778, 2016.
- Hertz, A., Mokady, R., Tenenbaum, J., Aberman, K., Pritch, Y., and Cohen-Or, D. Prompt-to-prompt image editing with cross attention control, 2022.
- Heusel, M., Ramsauer, H., Unterthiner, T., Nessler, B., and Hochreiter, S. Gans trained by a two time-scale update rule converge to a local nash equilibrium. *Advances in neural information processing systems*, 30, 2017.
- Ho, J., Jain, A., and Abbeel, P. Denoising diffusion probabilistic models. In Larochelle, H., Ranzato, M., Hadsell, R., Balcan, M., and Lin, H. (eds.), *Advances in Neural Information Processing Systems*, volume 33, pp. 6840–6851. Curran Associates, Inc., 2020. URL [https://proceedings.neurips.cc/paper\\_files/paper/2020/file/4c5bcfec8584af0d967f1ab10179ca4b-Paper.pdf](https://proceedings.neurips.cc/paper_files/paper/2020/file/4c5bcfec8584af0d967f1ab10179ca4b-Paper.pdf).
- Hu, E. J., Shen, Y., Wallis, P., Allen-Zhu, Z., Li, Y., Wang, S., Wang, L., and Chen, W. Lora: Low-rank adaptation of large language models, 2021.
- Hu, H. and Pang, J. Membership inference of diffusion models, 2023.
- Hu, Y., Wu, F., Li, Q., Long, Y., Garrido, G., Ge, C., Ding, B., Forsyth, D., Li, B., and Song, D. Sok: Privacy-preserving data synthesis. In *2024 IEEE Symposium on Security and Privacy (SP)*, pp. 2–2. IEEE Computer Society, 2023.
- Jiang, D., Zhang, G., Karami, M., Chen, X., Shao, Y., and Yu, Y. Dp<sup>2</sup>-vae: Differentially private pre-trained variational autoencoders. *arXiv preprint arXiv:2208.03409*, 2022.
- Karras, T., Aila, T., Laine, S., and Lehtinen, J. Progressive growing of GANs for improved quality, stability, and variation. In *International Conference on Learning Representations*, 2018. URL <https://openreview.net/forum?id=Hk99zCeAb>.
- Koh, P. W., Sagawa, S., Marklund, H., Xie, S. M., Zhang, M., Balsubramani, A., Hu, W., Yasunaga, M., Phillips, R. L., Gao, I., Lee, T., David, E., Stavness, I., Guo, W., Earnshaw, B. A., Haque, I. S., Beery, S., Leskovec, J., Kundaje, A., Pierson, E., Levine, S., Finn, C., and Liang, P. Wilds: A benchmark of in-the-wild distribution shifts, 2021.
- Krizhevsky, A., Hinton, G., et al. Learning multiple layers of features from tiny images. Technical report, University of Toronto, Toronto, ON, Canada, 2009.
- LeCun, Y. and Cortes, C. MNIST handwritten digit database. <http://yann.lecun.com/exdb/mnist/>, 2010. URL <http://yann.lecun.com/exdb/mnist/>.

- LeCun, Y., Bengio, Y., and Hinton, G. Deep learning. *nature*, 521(7553):436–444, 2015.
- Li, X., Tramer, F., Liang, P., and Hashimoto, T. Large language models can be strong differentially private learners. In *International Conference on Learning Representations*, 2022.
- Liew, S. P., Takahashi, T., and Ueno, M. PEARL: Data synthesis via private embeddings and adversarial reconstruction learning. In *International Conference on Learning Representations*, 2022a.
- Liew, S. P., Takahashi, T., and Ueno, M. PEARL: Data synthesis via private embeddings and adversarial reconstruction learning. In *International Conference on Learning Representations*, 2022b.
- Lin, Z., Gopi, S., Kulkarni, J., Nori, H., and Yekhanin, S. Differentially private synthetic data via foundation model apis 1: Images, 2023.
- Liu, Z., Luo, P., Wang, X., and Tang, X. Deep learning face attributes in the wild. In *Proceedings of International Conference on Computer Vision (ICCV)*, December 2015.
- Matsumoto, T., Miura, T., and Yanai, N. Membership inference attacks against diffusion models. In *2023 IEEE Security and Privacy Workshops (SPW)*, pp. 77–83, 2023. doi: 10.1109/SPW59333.2023.00013.
- Mohammed, N., Chen, R., Fung, B. C., and Yu, P. S. Differentially private data release for data mining. In *Proceedings of the 17th ACM SIGKDD International Conference on Knowledge Discovery and Data Mining*, KDD '11, pp. 493–501, New York, NY, USA, 2011. ACM. ISBN 978-1-4503-0813-7. doi: 10.1145/2020408.2020487.
- Papernot, N., Abadi, M., Erlingsson, U., Goodfellow, I. J., and Talwar, K. Semi-supervised knowledge transfer for deep learning from private training data. In *Proceedings of the International Conference on Learning Representations (ICLR)*, 2017.
- Park, D. H., Luo, G., Toste, C., Azadi, S., Liu, X., Karalashvili, M., Rohrbach, A., and Darrell, T. Shape-guided diffusion with inside-outside attention, 2023.
- Park, M., Foulds, J., Choudhary, K., and Welling, M. Dp-em: Differentially private expectation maximization. In *Artificial Intelligence and Statistics*, pp. 896–904. PMLR, 2017.
- Paszke, A., Gross, S., Massa, F., Lerer, A., Bradbury, J., Chanan, G., Killeen, T., Lin, Z., Gimelshein, N., Antiga, L., et al. Pytorch: An imperative style, high-performance deep learning library. *Advances in neural information processing systems*, 32, 2019.
- Pfutzner, B. and Arnrich, B. Dpd-fvae: Synthetic data generation using federated variational autoencoders with differentially-private decoder. *arXiv preprint arXiv:2211.11591*, 2022.
- Ponomareva, N., Vassilvitskii, S., Xu, Z., McMahan, B., Kurakin, A., and Zhang, C. How to dp-fy ml: A practical tutorial to machine learning with differential privacy. In *Proceedings of the 29th ACM SIGKDD Conference on Knowledge Discovery and Data Mining*, KDD '23, pp. 5823–5824, New York, NY, USA, 2023. Association for Computing Machinery. ISBN 9798400701030. doi: 10.1145/3580305.3599561. URL <https://doi.org/10.1145/3580305.3599561>.
- Qardaji, W., Yang, W., and Li, N. Priview: practical differentially private release of marginal contingency tables. In *Proceedings of the 2014 ACM SIGMOD international conference on Management of data*, pp. 1435–1446, 2014.
- Rombach, R., Blattmann, A., Lorenz, D., Esser, P., and Ommer, B. High-resolution image synthesis with latent diffusion models. In *Proceedings of the IEEE/CVF Conference on Computer Vision and Pattern Recognition (CVPR)*, pp. 10684–10695, June 2022.
- Ronneberger, O., Fischer, P., and Brox, T. U-net: Convolutional networks for biomedical image segmentation. In *Medical Image Computing and Computer-Assisted Intervention—MICCAI 2015: 18th International Conference, Munich, Germany, October 5-9, 2015, Proceedings, Part III* 18, pp. 234–241. Springer, 2015.
- Schuhmann, C., Vencu, R., Beaumont, R., Kaczmarczyk, R., Mullis, C., Katta, A., Coombes, T., Jitsev, J., and Komatsuzaki, A. Laion-400m: Open dataset of clip-filtered 400 million image-text pairs. *arXiv preprint arXiv:2111.02114*, 2021.
- Shi, B., Gai, S., Darrell, T., and Wang, X. Toast: Transfer learning via attention steering, 2023.
- Snoke, J. and Slavković, A. pmse mechanism: differentially private synthetic data with maximal distributional similarity. In *International Conference on Privacy in Statistical Databases*, pp. 138–159. Springer, 2018.
- Somepalli, G., Singla, V., Goldblum, M., Geiping, J., and Goldstein, T. Diffusion art or digital forgery? investigating data replication in diffusion models. In *Proceedings of the IEEE/CVF Conference on Computer Vision and Pattern Recognition (CVPR)*, pp. 6048–6058, June 2023.
- Song, Y., Sohl-Dickstein, J., Kingma, D. P., Kumar, A., Ermon, S., and Poole, B. Score-based generative modeling through stochastic differential equations. *International Conference on Learning Representations*, 2021.

- Tang, S., Wu, Z. S., Aydore, S., Kearns, M., and Roth, A. Membership inference attacks on diffusion models via quantile regression, 2023.
- Torkzadehmahani, R., Kairouz, P., and Paten, B. Dp-cgan: Differentially private synthetic data and label generation. In *The IEEE Conference on Computer Vision and Pattern Recognition (CVPR) Workshops*, June 2019.
- Tramèr, F., Kamath, G., and Carlini, N. Considerations for differentially private learning with large-scale public pretraining. *arXiv preprint arXiv:2212.06470*, 2022.
- Vaswani, A., Shazeer, N., Parmar, N., Uszkoreit, J., Jones, L., Gomez, A. N., Kaiser, Ł., and Polosukhin, I. Attention is all you need. *Advances in neural information processing systems*, 30, 2017.
- Vinaroz, M., Charusaie, M.-A., Harder, F., Adamczewski, K., and Park, M. J. Hermite polynomial features for private data generation. In *ICML*, volume 162 of *Proceedings of Machine Learning Research*, pp. 22300–22324. PMLR, 2022.
- Wu, Y., Yu, N., Li, Z., Backes, M., and Zhang, Y. Membership inference attacks against text-to-image generation models, 2023. URL <https://openreview.net/forum?id=J41IW8Z7mE>.
- Xia, W., Yang, Y., Xue, J.-H., and Wu, B. Tedigan: Text-guided diverse face image generation and manipulation. In *Proceedings of the IEEE/CVF conference on computer vision and pattern recognition*, pp. 2256–2265, 2021.
- Xiao, Y., Xiong, L., and Yuan, C. Differentially private data release through multidimensional partitioning. In *Secure Data Management*, pp. 150–168, Berlin, Heidelberg, 2010. Springer Berlin Heidelberg. ISBN 978-3-642-15546-8.
- Xie, L., Lin, K., Wang, S., Wang, F., and Zhou, J. Differentially private generative adversarial network. *arXiv preprint arXiv:1802.06739*, 2018.
- Yoon, J., Jordon, J., and van der Schaar, M. PATE-GAN: Generating synthetic data with differential privacy guarantees. In *International Conference on Learning Representations*, 2019.
- You, F. and Zhao, Z. Transferring pretrained diffusion probabilistic models, 2023. URL <https://openreview.net/forum?id=8u9eXwu5GAb>.
- Yousefpour, A., Shilov, I., Sablayrolles, A., Testuggine, D., Prasad, K., Malek, M., Nguyen, J., Ghosh, S., Bharadwaj, A., Zhao, J., Cormode, G., and Mironov, I. Opacus: User-friendly differential privacy library in PyTorch. *arXiv preprint arXiv:2109.12298*, 2021.
- Yu, D., Naik, S., Backurs, A., Gopi, S., Inan, H. A., Kamath, G., Kulkarni, J., Lee, Y. T., Manoel, A., Wutschitz, L., Yekhanin, S., and Zhang, H. Differentially private fine-tuning of language models. In *International Conference on Learning Representations*, 2022. URL <https://openreview.net/forum?id=Q42f0dfjECO>.
- Zagoruyko, S. and Komodakis, N. Wide residual networks, 2017.
- Zhang, J., Cormode, G., Procopiuc, C. M., Srivastava, D., and Xiao, X. Privbayes: Private data release via bayesian networks. *ACM Transactions on Database Systems (TODS)*, 42(4):1–41, 2017.
- Zhang, L., Rao, A., and Agrawala, M. Adding conditional control to text-to-image diffusion models, 2023a.
- Zhang, Q., Singh, C., Liu, L., Liu, X., Yu, B., Gao, J., and Zhao, T. Tell your model where to attend: Post-hoc attention steering for llms, 2023b.
- Zhang, Z., Wang, T., Li, N., Honorio, J., Backes, M., He, S., Chen, J., and Zhang, Y. Privsyn: Differentially private data synthesis. In *30th USENIX Security Symposium (USENIX Security 21)*, 2021.
- Zhu, T., Li, G., Zhou, W., and Yu, P. S. Differentially private data publishing and analysis: A survey. *IEEE Transactions on Knowledge and Data Engineering*, 29(8):1619–1638, August 2017. ISSN 1041-4347. doi: 10.1109/TKDE.2017.2697856.

## A. Additional Experiments

### A.1. Scaling factor effect in pre-training the autoencoder

In Table 6, we provide FID results after pre-training the autoencoder with Imagenet dataset for different scaling factors  $f$  and number of channels.

Table 6: FID scores (lower is better) for pre-trained autoencoders with different  $f$  and number of channels.

	# channels		
	128	64	32
$f = 2$	<b>27.6</b>	36.4	46.8
$f = 4$	32.9	51.0	83.5

### A.2. Transferring from EMNIST to MNIST distribution

Here are the details when we compare DP-LDM to existing methods with the most common DP settings  $\epsilon = 1, 10$  and  $\delta = 10^{-5}$  in Table 7.

Table 7: Downstream accuracies by CNN, MLP and WRN-40-4, evaluated on the generated MNIST data samples. We compare our results with existing work DPDM (Dockhorn et al., 2023), DP-Diffusion (Ghalebikesabi et al., 2023), PEARL (Liew et al., 2022b), DPGANr (Bie et al., 2022), and DP-HP (Vinaroz et al., 2022). The GPU hours is for DP training only. The GPU hours for pretraining steps of our method are present in Table 15 and Table 16.

		DP-LDM (Ours)	DP-DM	DP-Diffusion	DP-HP	PEARL	DPGANr
$\epsilon = 10$	CNN	97.4± 0.1	<b>98.1</b>	-	-	78.8	95.0
	WRN	97.5± 0.0	-	<b>98.6</b>	-	-	-
$\epsilon = 1$	CNN	<b>95.9± 0.1</b>	95.2	-	81.5	78.2	80.1
	# params	<b>0.8M</b>	1.75M	4.2M	-	-	-
	GPU Hours	<b>10h</b>	192h	-	-	-	-

#### A.2.1. CHOOSING PUBLIC DATASET WITH DP CONSTRAINT

FID scores are commonly used for measuring the similarity of two dataset. It first uses a pre-trained neural network (such as InceptionV3) to extract features from both datasets; then fits two Gaussian distributions to both datasets respectively, via computing the mean and covariance of the feature representations for both of them; then use the means and covariances to calculate the Fréchet distance. Following Park et al. (2017), we computed the FID scores between public data and private data in a differentially private manner. I.e. consider a data matrix by  $X$ , where  $n$  i.i.d. observations in a privacy-sensitive dataset are stacked in each row of  $X$ . We denote each observation of this dataset by  $\mathbf{x}_i \in \mathbb{R}^d$ . Hence,  $X \in \mathbb{R}^{n \times d}$ . We denote the inception feature given a datapoint  $\mathbf{x}_i$  by  $\phi(\mathbf{x}_i)$ . We further denote the mean and the covariance of the inception features, computed on a public dataset, by  $\mu_0$  and  $\Sigma_0$ . Similarly, we denote those computed on a privacy-sensitive dataset by  $\mu, \Sigma$ . The non-DP computation of FID is given by the following formula (notations are only used in this subsection):

$$\mathbf{FID} = \|\mu_0 - \mu\|_2^2 + \text{tr} \left[ \Sigma_0 + \Sigma - 2(\Sigma_0 \Sigma)^{\frac{1}{2}} \right]$$

We will need to privatize  $\mu$  and  $\Sigma$ . Following Park et al. (2017), we privatize the mean vector using a  $(\epsilon_1, \delta_1)$ -DP Gaussian mechanism. Let us first recall the definition of  $\mu$  given by :

$$\mu := \frac{1}{n} \sum_{i=1}^n \phi(\mathbf{x}_i).$$

Assuming  $\|\phi(\mathbf{x}_i)\| \leq 1$  for any  $i$ , the sensitivity of the mean vector denoted by  $\Delta_{\boldsymbol{\mu}}$  is :

$$\begin{aligned}\Delta_{\boldsymbol{\mu}} &= \max_{\mathbf{x}_j, \mathbf{x}'_j} \left\| \frac{1}{n} \left( \sum_{i \neq 1, i \neq j}^n \phi(\mathbf{x}_i) + \phi(\mathbf{x}_j) \right) - \frac{1}{n} \left( \sum_{i \neq 1, i \neq j}^n \phi(\mathbf{x}_i) + \phi(\mathbf{x}'_j) \right) \right\| \\ &= \frac{1}{n} \max_{\mathbf{x}_j, \mathbf{x}'_j} \|\phi(\mathbf{x}_j) - \phi(\mathbf{x}'_j)\| \\ &\leq \frac{1}{n} \cdot 2 \cdot \|\phi(\mathbf{x}_i)\| \\ &= 2/n\end{aligned}$$

i.e., bounded by  $2/n$ , when using the replacement definition of differential privacy (it is  $1/n$  when using the inclusion/exclusion definition of DP). Hence,

$$\tilde{\boldsymbol{\mu}} := \boldsymbol{\mu} + \mathbf{n}_1, \quad (4)$$

where  $\mathbf{n}_1$  is drawn from  $\mathcal{N}(0, \Delta_{\boldsymbol{\mu}}^2 \sigma_1^2 I)$ . Here,  $\sigma_1$  is a function of the privacy level given by  $(\epsilon_1, \delta_1)$ -DP. The exact relationship between  $\sigma_1$  and  $(\epsilon_1, \delta_1)$  varies depending on how to compute the DP bound. We use the bound introduced in the analytic Gaussian mechanism in <https://github.com/yuxiangw/autodp>.

Recall the definition of covariance given by:

$$\Sigma = \frac{1}{n} X^T X - \boldsymbol{\mu} \boldsymbol{\mu}^T.$$

Since we have a privatized mean from above, we need to privatize the second-moment matrix  $\frac{1}{n} X^T X = M_{\text{sec}}$  to privatize the covariance matrix.

As before, assuming  $\|\phi(\mathbf{x}_i)\| \leq 1, \forall i$ , the sensitivity of the second moment denoted by  $\Delta_{M_{\text{sec}}}$  is :

$$\begin{aligned}\Delta_{M_{\text{sec}}} &= \max_{\phi(\mathbf{x}_j), \phi(\mathbf{x}'_j)} \left\| \frac{1}{n} \left( \sum_{i \neq 1, i \neq j}^n \phi(\mathbf{x}_i) \phi(\mathbf{x}_i^T) + \phi(\mathbf{x}_j) \phi(\mathbf{x}_j^T) \right) - \frac{1}{n} \left( \sum_{i \neq 1, i \neq j}^n \phi(\mathbf{x}_i) \phi(\mathbf{x}_i^T) + \phi(\mathbf{x}'_j) \phi(\mathbf{x}'_j^T) \right) \right\|_F \\ &= \frac{1}{n} \max_{\phi(\mathbf{x}_j), \phi(\mathbf{x}'_j)} \|\phi(\mathbf{x}_j) \phi(\mathbf{x}_j^T) - \phi(\mathbf{x}'_j) \phi(\mathbf{x}'_j^T)\|_F \\ &\leq \frac{2}{n} \max_{\phi(\mathbf{x}_j)} \|\phi(\mathbf{x}_j) \phi(\mathbf{x}_j^T)\|_F \quad (\text{WLOG, say } \|\phi(\mathbf{x}'_j) \phi(\mathbf{x}'_j^T)\|_F \leq \|\phi(\mathbf{x}_j) \phi(\mathbf{x}_j^T)\|_F) \\ &= \frac{2}{n} \max_{\phi(\mathbf{x}_j)} \sqrt{\sum_{i=1}^d \sum_{k=1}^d |\alpha_i \alpha_k|^2} \quad (\text{Say } \phi(\mathbf{x}_j) = [\alpha_1, \dots, \alpha_d] \text{ as a column vector}) \\ &= \frac{2}{n} \max_{\phi(\mathbf{x}_j)} \sqrt{\sum_{i=1}^d (\alpha_i^2 \cdot \sum_{k=1}^d \alpha_k^2)} \\ &= \frac{2}{n} \max_{\phi(\mathbf{x}_j)} \sqrt{\left( \sum_{i=1}^d \alpha_i^2 \right) \cdot \left( \sum_{k=1}^d \alpha_k^2 \right)} \\ &= \frac{2}{n} \max_{\phi(\mathbf{x}_j)} \sqrt{\|\phi(\mathbf{x}_j)\|_2^2 \cdot \|\phi(\mathbf{x}_j)\|_2^2} \\ &\leq \frac{2}{n}\end{aligned}$$

i.e., bounded by  $2/n$ , when using the replacement definition of differential privacy (it is  $1/n$  when using the inclusion/exclusion definition of DP). See eq(17) in [Park et al. \(2017\)](#) for derivation of the sensitivity.

Given a privacy budget  $(\epsilon_2, \delta_2)$ -DP assigned to this privatization step, which gives us a corresponding privacy parameter  $\sigma_2$ , we first draw noise  $\mathbf{n}_2$  from  $\mathcal{N}(0, \Delta_{M_{\text{sec}}}^2 \sigma_2^2 I_{d(d+1)/2})$ . We then add this noise to the upper triangular part of the matrix,

Table 8: Left : Perturbed FIDs when privatizing both mean and covariance. Note  $\epsilon$  listed is the sum of  $\epsilon_\mu + \epsilon_\Sigma$ , we take  $\epsilon_\mu = \epsilon_\Sigma$ . Right : Perturbed mean differences when privatizing mean only.  $\epsilon$  listed is  $\epsilon_\mu$

$\epsilon$	0.1	0.5	1	2	5	10	$\epsilon$	0.1	0.5	1	2
SVHN	<b>78.9930</b>	<b>17.3465</b>	8.9223	4.7426	2.1582	1.3368	SVHN	0.2675	0.2662	0.2663	0.2663
KMNIST	79.9224	17.5794	9.0605	4.6092	1.9300	1.0794	KMNIST	0.0489	0.0459	0.0457	0.0457
EMNIST	80.4267	17.3617	<b>8.9058</b>	<b>4.4561</b>	<b>1.8926</b>	<b>1.0242</b>	EMNIST	<b>0.0228</b>	<b>0.0201</b>	<b>0.0201</b>	<b>0.0197</b>

including the diagonal component. To ensure the symmetry of the perturbed second-moment matrix  $\widetilde{M}_{\text{sec}}$ , we copy the noise added to the upper triangular part and add one by one to the lower triangular part. We then obtain

$$\widetilde{\Sigma} = \widetilde{M}_{\text{sec}} - \widetilde{\mu}\widetilde{\mu}^T. \quad (5)$$

Note  $\widetilde{\Sigma}$  may not be positive definite. In such a case, we can project the negative eigenvalue to some small value close to zero to guarantee the positive definite property of the covariance matrix. This is safe to do, as DP is post-processing invariant.

Using the aforementioned privatized mean given in (4) and covariance given in (5), we can compute the final FID score, given by

$$\text{DP-FID} = \|\mu_0 - \widetilde{\mu}\|_2^2 + \text{tr} \left[ \Sigma_0 + \widetilde{\Sigma} - 2 \left( \Sigma_0 \widetilde{\Sigma} \right)^{\frac{1}{2}} \right],$$

which is  $(\epsilon_1 + \epsilon_2, \delta_1 + \delta_2)$ -DP.

Following the above method, we compute the DP-FID scores of SVHN, KMNIST, and EMNIST, with respect to private dataset MNIST. We sampled 60k data from each public dataset candidates to do a fair comparison, the results are in Table 8 left. One could consider only privatizing the mean only, and the results are in Table 8 right. Based on these results, we choose EMNIST as a public dataset.

#### A.2.2. ADDITIONAL EXPERIMENTS WITH SVHN AND KMNIST

To verify our choice of EMNIST empirically, we also did ablation experiments on SVHN and KMNIST under the same privacy condition  $\epsilon = 10, \delta = 10^{-5}$  to compare with EMNIST, the results are illustrated in Table 9.

Table 9: We also pretrained LDMs using SVHN and KMNIST then fine-tuned with MNIST, and list the CNN accuracy here respectively.

Dataset pair	CNN accuracy
(SVHN, MNIST)	94.3
(KMNIST, MNIST)	96.3
<b>(EMNIST, MNIST)</b>	<b>97.4</b>

#### A.2.3. ABLATION EXPERIMENTS FOR MNIST

There are 7 attention modules in the Unet structure for MNIST, 1-2 are in input\_blocks, 3 is in middle\_block, 4-7 are in out\_blocks as illustrated in Fig. 5. Modules in blue are frozen during fine-tuning. Parameters of condition embedder is always trained. We consider fine tune only  $i$ -th to 7th attention modules to reduce more trainable parameters. Results for  $\epsilon = 10, \delta = 10^{-5}$  are listed in Table 10. The best results is achieved when fine tune with 4-7 attention blocks, which means out\_blocks are more important than others during training.

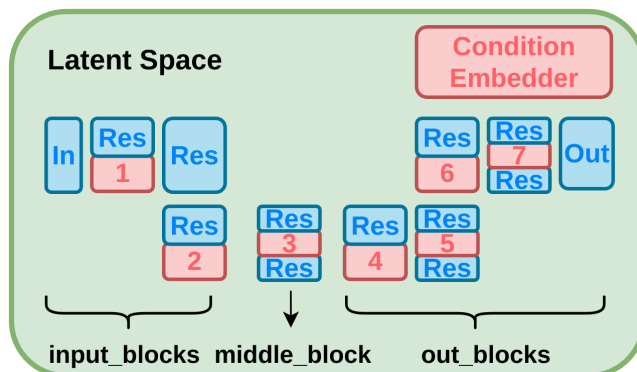


Figure 5: Unet Structure for MNIST.

Table 10: CNN accuracy and number of trainable parameters for MNIST ablation experiments with varying number of fine-tuning layers. Privacy condition is set to  $\epsilon = 10, \delta = 10^{-5}$ .

	1-7(all)	2-7	3-7	4-7	5-7
CNN	97.3	97.3	90	<b>97.4</b>	97.3
# of trainable params	1.6M	1.5M	1.2M	0.8M	0.5M
out of 4.6M total params	(34.3%)	(32.4%)	(25.2%)	(18.0%)	(10.9%)

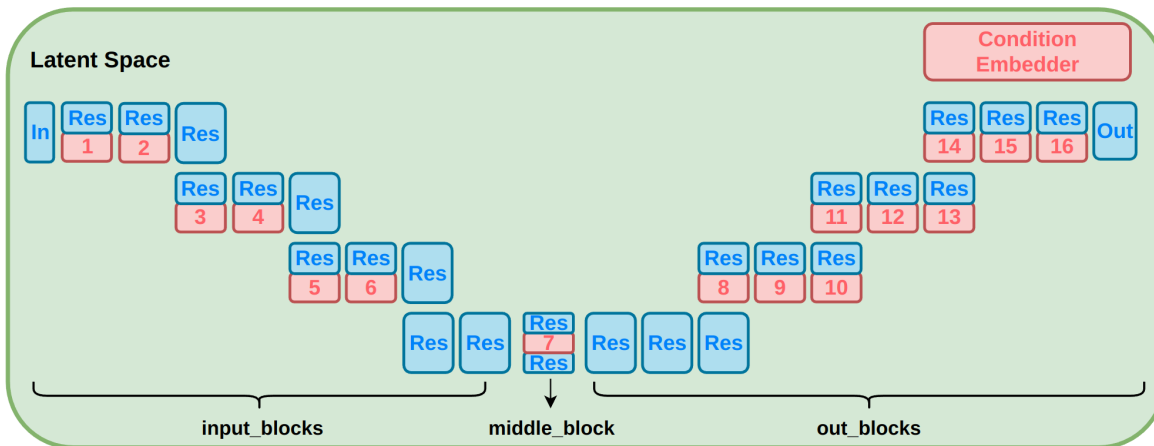


Figure 6: Unet Structure for CIFAR-10

### A.3. Transferring from Imagenet to CIFAR10 distribution

Here, we provide the results for ablation experiments to test the performance of DP-LDM when fine-tuning only certain attention modules inside the pre-trained model and keeping the rest of the parameters fixed. There are 16 attention modules in total as illustrated in Fig. 6. Table 11 shows the FID obtained for  $\epsilon = 1, 5, 10$  and  $\delta = 10^{-5}$  for the different number of attention modules fine-tuned. The results show that fixing up to the first half of the attention layers in the LDM has a positive effect in terms of the FID (the lower the better) in our model.

Table 11: FID scores (lower is better) for synthetic CIFAR-10 data with varying the number of fine-tuning layers and privacy guarantees. **Top row (1-16 layers):** Fine-tuning all attention modules. **Second row (5-16 layers):** Keep first 4 attention modules fixed and fine-tuning from 5 to 16 attention modules. **Third row (9-16 layers):** Keep first 8 attention modules fixed and fine-tuning from 9 to 16 attention modules. **Bottom row (13-16 layers):** Keep first 12 attention modules fixed and fine-tuning from 13 to 16 attention modules.

DP-LDM	$\epsilon = 10$	$\epsilon = 5$	$\epsilon = 1$
1-16 layers	25.8 ± 0.3	29.9 ± 0.2	33.0 ± 0.3
5 - 16 layers	15.7 ± 0.3	21.2 ± 0.2	28.9 ± 0.2
9 - 16 layers	<b>8.4 ± 0.2</b>	<b>13.4 ± 0.4</b>	<b>22.9 ± 0.5</b>
13 - 16 layers	12.3 ± 0.2	18.5 ± 0.2	25.2 ± 0.5

We also report the different hyper-parameter settings used in ablation experiments in table Table 12.

Table 13 shows the hyper-parameters used during training ResNet9 and WRN40-4 downstream classifiers on CIFAR10 synthetic samples.

### A.4. Transferring from Imagenet to CelebA32

We also apply our model in the task of generating  $32 \times 32$  CelebA images. The same pretrained autoencoder as our CIFAR-10 experiments in Section 5.1 is used, but since this experiment is for unconditional generation, we are unable to



Table 12: DP-LDM hyper-parameter setting on CIFAR-10 for different ablation experiments.

		$\epsilon = 10$	$\epsilon = 5$	$\epsilon = 1$
1-16 layers (24.4M parameters)	batch size	1000	2000	1000
	clipping norm	$10^{-5}$	$10^{-5}$	$10^{-3}$
	learning rate	$10^{-6}$	$10^{-6}$	$10^{-6}$
	epochs	30	30	10
5-16 layers (20.8M parameters)	batch size	5000	5000	2000
	clipping norm	$10^{-6}$	$10^{-5}$	$10^{-3}$
	learning rate	$10^{-6}$	$10^{-6}$	$10^{-5}$
	epochs	50	50	10
9-16 layers (10.2M parameters)	batch size	2000	2000	5000
	clipping norm	$10^{-6}$	$10^{-6}$	$10^{-2}$
	learning rate	$10^{-6}$	$10^{-6}$	$10^{-6}$
	epochs	30	30	10
13-16 layers (4M parameters)	batch size	2000	2000	2000
	clipping norm	$10^{-6}$	$10^{-6}$	$10^{-2}$
	learning rate	$10^{-6}$	$10^{-6}$	$10^{-6}$
	epochs	30	30	10

Table 13: Hyperparameters for downstream classification ResNet9 and WRN40-4 trained on CIFAR10 synthetic data

	ResNet9	WRN40-4
learning rate	0.5	0.1
batch size	512	1000
epochs	10	10000
optimizer	SGD	SGD
label smoothing	0.1	0.0
weight decay	$5 \cdot 10^{-4}$	$5 \cdot 10^{-4}$
momentum	0.9	0.9

re-use the LDM. A new LDM is pretrained on Imagenet without class conditioning information, and then fine-tuned on CelebA images scaled and cropped to  $32 \times 32$  resolution. Our FID results for  $\delta = 10^{-6}$ ,  $\epsilon = 1, 5, 10$  are summarized in Table 14. We achieve similar results to DP-MEPF for  $\epsilon = 5$  and  $\epsilon = 10$ . As with our results at  $64 \times 64$  resolution, our LDM model does not perform as well in higher privacy settings ( $\epsilon = 1$ ). Sample images are provided in Figure 7

### A.5. Transferring from Imagenet to Camelyon17-WILDS

Camelyon17-WILDS is part of the WILDS benchmark suite of datasets, containing 455,954 medical images at  $96 \times 96$  resolution. The downstream task is to determine whether the center  $32 \times 32$  patch of the image contains any tumor pixels. In our experiment, we crop the image so that only the center  $32 \times 32$  patch is passed to the model. We begin with the same pretrained autoencoder and LDM as in our CIFAR-10 experiments (Section 5.1), and fine-tune on Camelyon17-WILDS. We then generate 25,000 images conditioned on each of the two classes, and combine them to create a synthetic dataset of 50,000 images. Finally, the synthetic dataset is used to train a WRN-40-4 classifier.

## B. Hyperparameters

Here we provide an overview of the hyperparameters of the pretrained autoencoder in Table 15, hyperparameters of the pretrained diffusion models in Table 16. Note that *base learning rate* is the one set in the yaml files. The real learning rate passed to the optimizer is  $accumulate\_grad\_batches \times num\_gpus \times batch\_size \times base\_learning\_rate$ .

Table 17 shows the hyperparameters we used for fine-tuning on MNIST. Table 18 shows the hyperparameters we used for CelebA32. Table 19 shows the hyperparameters we used for CelebA64. Table 21 shows the hyperparameters we used

Table 14: CelebA FID scores (lower is better) for images of resolution  $32 \times 32$  comparing with results from DPDM (Dockhorn et al., 2023), DP Sinkhorn (Cao et al., 2021), and DP-MEPF (Harder et al., 2023).

	$\epsilon = 10$	$\epsilon = 5$	$\epsilon = 1$
<b>DP-LDM</b> (ours, average)	$16.2 \pm 0.2$	$16.8 \pm 0.3$	$25.8 \pm 0.9$
<b>DP-LDM</b> (ours, best)	<b>16.1</b>	<b>16.6</b>	24.6
DP-MEPF ( $\phi_1$ )	16.3	17.2	<b>17.2</b>
DP-GAN (pre-trained)	58.1	66.9	81.3
DPDM (no public data)	21.2	-	71.8
DP Sinkhorn (no public data)	189.5	-	-

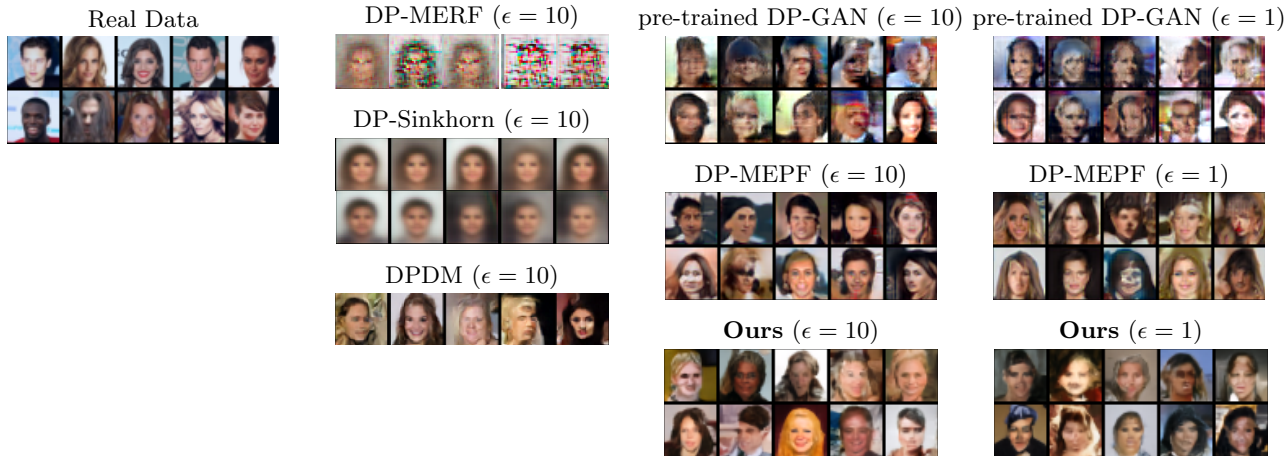


Figure 7: Synthetic  $32 \times 32$  CelebA samples generated at different levels of privacy. Samples for DP-MERF and DP-Sinkhorn are taken from (Cao et al., 2021), DPDM samples are taken from (Dockhorn et al., 2023), and DP-MEPF samples are taken from (Harder et al., 2023).

for text-to-image CelebAHQ generation. Table 22 shows the hyperparameters we used for class-conditioned CelebAHQ generation.

### C. Additional Samples

Table 15: Hyperparameters for the pretrained autoencoders for different datasets.

	EMNIST (to MNIST)	ImageNet (to CIFAR10)	ImageNet (to CelebA 32)	ImageNet (to CelebA 64)
Input size	32	32	32	64
Latent size	4	16	16	32
$f$	8	2	2	2
$z$ -shape	$4 \times 4 \times 3$	$16 \times 16 \times 3$	$16 \times 16 \times 3$	$64 \times 64 \times 3$
Channels	128	128	128	192
Channel multiplier	[1,2,3,5]	[1,2]	[1,2]	[1,2]
Attention resolutions	[32,16,8]	[16, 8]	[16, 8]	[16,8]
num_res.blocks	2	2	2	2
Batch size	50	16	16	16
Base learning rate	$4.5 \times 10^{-6}$	$4.5 \times 10^{-6}$	$4.5 \times 10^{-6}$	$1.0 \times 10^{-6}$
Learning rate	$4.5 \times 10^{-4}$	$1.4 \times 10^{-4}$	$1.4 \times 10^{-4}$	$1.4 \times 10^{-4}$
Epochs	50	2	2	-
GPU(s)	1 NVIDIA V100	1 NVIDIA RTX A4000	1 NVIDIA RTX A4000	1 NVIDIA V100
Time	8 hours	1 day	1 day	1 day

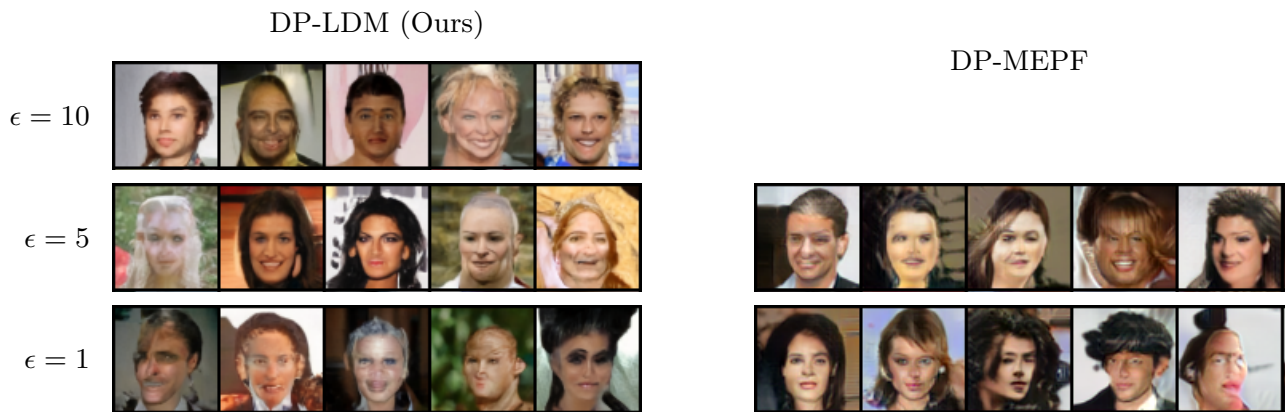


Figure 8: Synthetic  $64 \times 64$  CelebA samples generated at different levels of privacy. Samples for DP-MEPF are taken from Harder et al. (2023).

Table 16: Hyperparameters for the pretrained diffusion models for different datasets.

	EMNIST (to MNIST)	ImageNet (to CIFAR10)	ImageNet (to CelebA 32)	ImageNet (to CelebA64)
input size	32	32	32	64
latent size	4	16	16	32
$f$	8	2	2	2
$z$ -shape	$4 \times 4 \times 3$	$16 \times 16 \times 3$	$16 \times 16 \times 3$	$32 \times 32 \times 3$
channels	64	128	192	192
channel multiplier	[1,2]	[1,2,2,4]	[1,2,4]	[1,2,4]
attention resolutions	[1,2]	[1,2,4]	[1,2,4]	[1,2,4]
num_res_blocks	1	2	2	2
num_heads	2	8	-	8
num_head_channels	-	-	32	-
batch size	512	500	384	256
base learning rate	$5 \times 10^{-6}$	$1 \times 10^{-6}$	$5 \times 10^{-7}$	$1 \times 10^{-6}$
learning rate	$2.6 \times 10^{-3}$	$5 \times 10^{-4}$	$2 \times 10^{-4}$	$2.6 \times 10^{-4}$
epochs	120	30	13	40
# trainable parameters	4.6M	90.8M	162.3M	72.2M
GPU(s)	1 NVIDIA V100	1 NVIDIA RTX A4000	1 NVIDIA V100	1 NVIDIA V100
time	6 hours	7 days	30 hours	10 days
use_spatial_transformer	True	True	False	False
cond_stage_key	class_label	class_label	-	-
conditioning_key	crossattn	crossattn	-	-
num_classes	26	1000	-	-
embedding dimension	5	512	-	-
transformer depth	1	1	-	-

Table 17: Hyperparameters for fine-tuning diffusion models with DP constraints  $\epsilon = 10, 1$  and  $\delta = 10^{-5}$  on MNIST. The “ablation” hyperparameter determines which attention modules are fine-tuned, where a value of  $i$  means that the first  $i - 1$  attention modules are frozen and others are trained. Setting “ablation” to  $-1$  (default) fine-tunes all attention modules.

	$\epsilon = 10$	$\epsilon = 1$
batch size	2000	2000
base learning rate	$5 \times 10^{-7}$	$6 \times 10^{-7}$
learning rate	$1 \times 10^{-3}$	$1.2 \times 10^{-3}$
epochs	200	200
clipping norm	0.01	0.001
noise scale	1.47	9.78
ablation	4	-1
num of params	0.8M	1.6M
use_spatial_transformer	True	True
cond_stage_key	class_label	class_label
conditioning_key	crossattn	crossattn
num_classes	26	26
embedding dimension	13	13
transformer depth	1	1
train_condition_only	True	True
attention_flag	spatial	spatial
# condition params	338	338

Table 18: Hyperparameters for fine-tuning diffusion models with DP constraints  $\epsilon = 10, 5, 1$  and  $\delta = 10^{-6}$  on CelebA32.

	$\epsilon = 10$	$\epsilon = 5$	$\epsilon = 1$
batch size	8192	8192	2048
base learning rate	$5 \times 10^{-7}$	$5 \times 10^{-7}$	$5 \times 10^{-7}$
learning rate	$4 \times 10^{-3}$	$4 \times 10^{-3}$	$1 \times 10^{-3}$
epochs	20	20	20
clipping norm	$5.0 \times 10^{-4}$	$5.0 \times 10^{-4}$	$5.0 \times 10^{-4}$
ablation	-1	-1	-1
use_spatial_transformer	False	False	False
cond_stage_key	-	-	-
conditioning_key	-	-	-
num_classes	-	-	-
embedding dimension	-	-	-
transformer depth	-	-	-
train_attention_only	True	True	True

Table 19: Hyperparameters for fine-tuning diffusion models with DP constraints  $\epsilon = 10, 5, 1$  and  $\delta = 10^{-6}$  on CelebA64.

	$\epsilon = 10$	$\epsilon = 5$	$\epsilon = 1$
batch size	8192	8192	8192
base learning rate	$1 \times 10^{-7}$	$1 \times 10^{-7}$	$1 \times 10^{-7}$
learning rate	$8.2 \times 10^{-4}$	$8.2 \times 10^{-4}$	$8.2 \times 10^{-4}$
epochs	70	70	70
clipping norm	$5.0 \times 10^{-4}$	$5.0 \times 10^{-4}$	$5.0 \times 10^{-4}$
ablation	-1	-1	-1
use_spatial_transformer	False	False	False
cond_stage_key	-	-	-
conditioning_key	-	-	-
num_classes	-	-	-
embedding dimension	-	-	-
transformer depth	-	-	-
train_attention_only	True	True	True

Table 20: Hyperparameters for fine-tuning diffusion models with DP constraint  $\epsilon = 10$  and  $\delta = 3 \times 10^{-6}$  on Camelyon17-WILDS.

	$\epsilon = 10$
batch size	20000
base learning rate	$1.0 \times 10^{-7}$
learning rate	$2.0 \times 10^{-3}$
epochs	30
clipping norm	$1.0 \times 10^{-6}$
ablation	13
use_spatial_transformer	True
cond_stage_key	class_label
conditioning_key	crossattn
num_classes	1001
embedding dimension	512
transformer depth	1
train_condition_only	True
attention_flag	spatial
# condition params	512, 512

Table 21: Hyperparameters for fine-tuning diffusion models with DP constraints  $\epsilon = 10, 1$  and  $\delta = 10^{-5}$  on text-conditioned CelebAHQ.

	$\epsilon = 10$	$\epsilon = 1$
batch size	256	256
base learning rate	$1 \times 10^{-7}$	$1 \times 10^{-7}$
learning rate	$2.6 \times 10^{-5}$	$2.6 \times 10^{-5}$
epochs	10	10
clipping norm	0.01	0.01
noise scale	0.55	1.46
ablation	-1	-1
num of params	280M	280M
use_spatial_transformer	True	True
cond_stage_key	caption	caption
context_dim	1280	1280
conditioning_key	crossattn	crossattn
transformer depth	1	1

Table 22: Hyperparameters for fine-tuning diffusion models with DP constraints  $\epsilon = 10, 5, 1$  and  $\delta = 10^{-5}$  on class-conditional CelebAHQ.

	$\epsilon = 10$	$\epsilon = 5$	$\epsilon = 1$
batch size	2048	2048	2048
base learning rate	$1 \times 10^{-7}$	$1 \times 10^{-7}$	$1 \times 10^{-7}$
learning rate	$2.0 \times 10^{-4}$	$2.0 \times 10^{-4}$	$2.0 \times 10^{-4}$
epochs	50	50	50
clipping norm	$5.0 \times 10^{-4}$	$5.0 \times 10^{-4}$	$5.0 \times 10^{-4}$
ablation	-1	-1	-1
use_spatial_transformer	True	True	True
cond_stage_key	class_label	class_label	class_label
context_dim	512	512	512
conditioning_key	crossattn	crossattn	crossattn
transformer depth	1	1	1